





Connecting Networks for Two-Dimensional Butler Matrices Generating a Triangular Lattice of Beams

NELSON J. G. FONSECA ¹ (Senior Member, IEEE), SOPHIE-ABIGAE GOMANNE¹,
PILAR CASTILLO-TAPIA² (Graduate Student Member, IEEE),
OSCAR QUEVEDO-TERUEL ² (Senior Member, IEEE), TAKASHI TOMURA ³ (Senior Member, IEEE),
AND JIRO HIROKAWA ³ (Fellow, IEEE)

(Invited Paper)

¹Antenna and Sub-Millimetre Waves Section, European Space Agency, 2200, AG Noordwijk, The Netherlands

²Division of Electromagnetic Engineering, KTH Royal Institute of Technology, SE-11428 Stockholm, Sweden

³Department of Electrical and Electronic Engineering, Tokyo Institute of Technology, Tokyo 152-8550, Japan

CORRESPONDING AUTHOR: N. J. G. Fonseca (e-mail: nelson.fonseca@esa.int).

This work was supported by the European Space Agency in the frame of the Technology Transfer Contract 4000130375/20/NL. The work of Oscar Quevedo-Teruel and Pilar Castillo-Tapia was also supported by the VR Project 2019-03933 under call "Research project grant within natural and engineering sciences."

ABSTRACT Connecting networks for two-dimensional beamforming matrices are discussed. They provide a suitable interconnection between the output ports of a Butler matrix and antenna array ports, transforming a square (and more generally, rectangular) lattice of beams into a triangular lattice of beams. This change in lattice improves the crossover between beams, reducing gain roll-off over the field of view for a given multiple fixed beam coverage. A general description of the concept is provided and numerical results are reported, which confirm a reduction in crossover level between 1 and 1.5 dB. The proposed solution is further validated through the design and test of a 4×4 open-ended waveguide array in K-band. The connecting network has a length of 70 mm, compared to 226 mm for the 2D Butler matrix, with a design frequency of 19.55 GHz. Good agreement is found between simulated and measured data. The desired triangular lattice of beams is confirmed with the measured multiple beams. This solution is of interest for multiple-beam millimeter-wave communication systems, considered for next generation of terrestrial and non-terrestrial networks.

INDEX TERMS Beamforming networks, multiple fixed beam antenna, open-ended waveguide arrays, triangular lattice of beams, two-dimensional Butler matrix.

I. INTRODUCTION

In recent years, there have been various developments reported on multiple beam antennas and associated beamforming techniques, driven by the specific needs of 5G terrestrial networks as well as small-space platforms for low Earth orbit (LEO) satellite constellations. This includes advances on beam forming networks (BFN), such as Blass [1], [2], Butler [3]–[5] and Nolen matrices [6]–[8], as well as parallel plate waveguide quasi-optical beamformers [9]–[14]. When a small number of beams is required (typically a few tens of beams), BFNs are generally preferred, and in particular Butler matrices in waveguide technology,

as they provide low insertion losses and higher integration in the millimeter-wave band. However, Butler matrices only provide one-dimensional (1D) beamforming in their standard form. Planar arrays require an arrangement of two orthogonal stacks of Butler matrices [3]. An alternative solution consists in using two-dimensional (2D) components, such as couplers and crossovers, to reduce the over length of the BFN by combining the two stages of 1D beamforming into a direct 2D beamforming approach [15]. The performance of 16×16 and 64×64 2D Butler matrices are detailed in [16], [17]. Because of its topology, this 2D BFN inherently generates a square lattice of beams. Actually, even a standard two-stack of

1D Butler matrices would generate a similar lattice of beams. This topology is not optimal for multiple beam or switched beam applications as the gain roll-off over the antenna field of view is typically between 7 and 8 dB, excluding scan losses, with the worst-case angular direction being at the intersection of four adjacent beams in a square lattice. This value can be reduced using a triangular lattice instead, in which the worst-case corresponds to the intersection of three adjacent beams. Minimizing the gain roll-off of the antenna system over the service area is critical as multiple beam communication systems are constrained on the lower end by the link budget requiring to maximize the worst-case aggregate gain value, and on the upper end, by a maximum allowed power flux density setting an upper limit on the aggregate gain.

Despite obvious benefits in terms of performance, only a limited number of array antenna solutions generating a triangular lattice of beams with Butler matrices (and more generally, linear beamformers) have been discussed in the literature. The first solution, reported back in the 1960s, consists in using oversized 1D Butler matrices with a suitable array-matrix interconnection [19]. However, its extension to 2D Butler matrices is not straightforward. In fact, the proposed configuration generating a triangular lattice of beams is referred to as a “degenerate” matrix, meaning that it requires multiple 1D Butler matrices of smaller size. Unfortunately, their interconnection, which is significant to the overall BFN design and performance, is not detailed in that contribution. The numerical results reported, based on array factor analyses, indicate an improvement in beam crossover level from -7.5 to -5.9 dB by changing from a square lattice to a triangular lattice without changing the array layout, while keeping the BFN orthogonal (i.e. theoretically lossless [20], [21]). A complete solution based on 1D Butler matrices was eventually proposed three decades later [22]. It uses a standard two-stack arrangement and adds adequate phase gradients in between the two stacks so as to shift every second line of beams by half-a-beamwidth, thus turning the square lattice into a triangular lattice of beams. This may be seen as an implementation of the general concept described by Shelton [19], where a N^2 array is fed by a “degenerate” $N^2 \times N^2$ 1D Butler matrix, which requires two $N^2/2 \times N^2/2$ Butler matrices, each producing a rectangular lattice of beams shifted along one axis by half-a-beamwidth with respect to each other. Those two matrices may eventually be decomposed into N matrices of size $N \times N$, where N is a power of two, thus providing the first stack of 1D Butler matrices in a standard two-stack arrangement. The second stack, modified with the added phase gradients as proposed in [22], provides the desired property. A similar approach is demonstrated in [23] using two stacks of Rotman lenses [24]. The two different phase gradients required in the first stage of beamforming are obtained directly by adjusting the location of the feeds in the Rotman lenses, thus simplifying the overall design and assembly. This solution also works with a stack of linear arrays in front of a doubly curved reflector [25]–[27]. Although their simplicity is attractive, these solutions are not compatible with a 2D Butler matrix since

they require the 2D beamforming to be implemented in two separate 1D beamforming stages. A possible solution is the approach described in [28] with two stacks of Rotman lenses. However, this method requires to load a number of output ports, adding losses to the design.

A new approach, revisiting the concept of array-matrix interconnection, was introduced in [29]. The proposed connecting network is adapted to the specific topology of a 2D Butler matrix. This approach was inspired by a property used in [30] to reduce side lobe level in Butler matrices, recently revisited and applied to Nolen matrices [31]. This paper provides a thorough description of the proposed connecting network solution, supported by an experimental validation. The general concept is first detailed in Section II. A practical design in waveguide technology, compatible with a 2D Butler matrix in K-band [15], is described in Section III, also including experimental results. Section IV provides some conclusions and directions for future works.

II. CONNECTING NETWORKS FOR 2D MATRICES

A. PRINCIPLE OF OPERATION

The key feature of the proposed connecting networks is to make the suitable interconnection between a 2D Butler matrix having a square (or rectangular) lattice of ports and an array generating a triangular lattice of beams with reduced beam crossover level. Without lack of generality, the concept is described here in the case of a 16-element array (4×4 planar array) and associated 16×16 Butler matrix. The extension of the concept to any size of 2D Butler matrix is straightforward from the development that follows. Note also that it is described here in connection with 2D Butler matrices, but it could be extended to other types of 2D BFNs, including those formed with two stacks of 1D BFNs, provided they are orthogonal [4], [20], [21].

Using an approach similar to the one described in [28], the first step is to change the original square lattice of the matrix (Fig. 1 a) into a triangular array lattice (Fig. 1b). With the 2D phase progressions provided by the Butler matrix, this will automatically produce a triangular lattice of beams, as the beam axes in the (u, v) representation are orthogonal to the (x, y) -axes of the array, where $u = \sin \theta \cos \phi$ and $v = \sin \theta \sin \phi$, the angles (θ, ϕ) being the conventional spherical coordinates in (x, y, z) [32]. However, the resulting diamond-like array shape produces elliptical beams and beam crossover does not improve. Contour plots are provided for both the square array and the diamond array in Fig. 2a and 2b respectively, using the same assumptions as in [16]. These results are obtained at 22 GHz for arrays of open-ended rectangular waveguides with a spacing $d = 9.9$ mm and aperture dimensions $a = 7.9$ mm and $b = 4.4$ mm, corresponding to the array configuration also used in [29]. The *solid line* contours (1 and 3.9 dB below the peak of each beam) correspond to the array performance accounting for element coupling and edge effects due to the finite size of the ground plane (minimum edge dimension for the designs considered is 50 mm), while the *dotted red line*

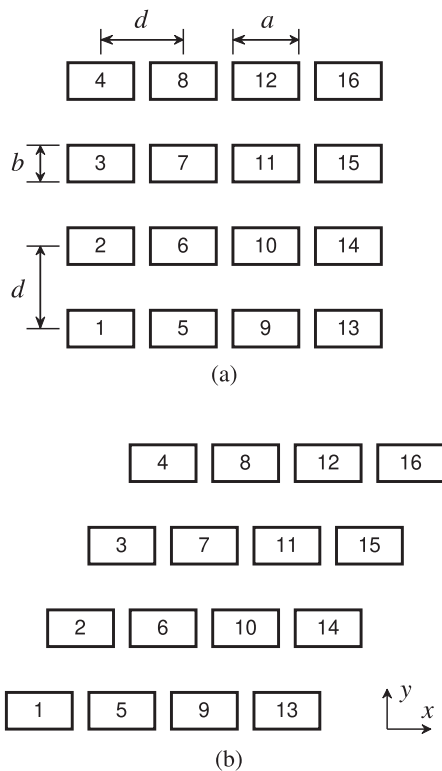


FIGURE 1. Design parameters and layout of (a) a 4×4 square array and (b) a 4×4 diamond array.

contours (3.9 dB below the peak only) correspond to ideal array performance (array factor combined with ideal array element patterns) for direct comparison with the analyses reported in [19]. A value of 3.9 dB below the peak is considered here as benchmark as this corresponds to the typical cross-over level between adjacent beams in orthogonal linear beamforming networks. The array models, analyzed using ANSYS HFSS, are reported as insets in Fig. 2. The worst-case beam crossover is -7.1 dB and -7.5 dB for respectively the ideal square array and the ideal diamond array. The values drop to respectively -7.9 dB and -8.1 dB for the full-wave array models. This change in crossover level is due to mutual coupling and edge effects which tend to increase the array element directivity. This is particularly visible in Fig. 2 where grating lobes appear along the u -axis for the ideal array (*dotted red line* contours beyond the nominal 4×4 beam lattice), as the open-ended rectangular waveguides provide different beamwidths in the two main planes. The grating lobes are lowered below the contour levels reported in the case of the full-wave array models. The trend is the same for both arrays. These results confirm that simply changing the lattice is not sufficient to improve the beam crossover level. This problem was solved in [28] by loading some of the array elements to obtain a hexagonal array shape, providing beams with more circular contour levels in the (u, v) space. However, the improvement of about 1 to 1.5 dB in gain roll-off comes at the expense of a similar loss in gain, which is not desirable when working with theoretically lossless BFNs.

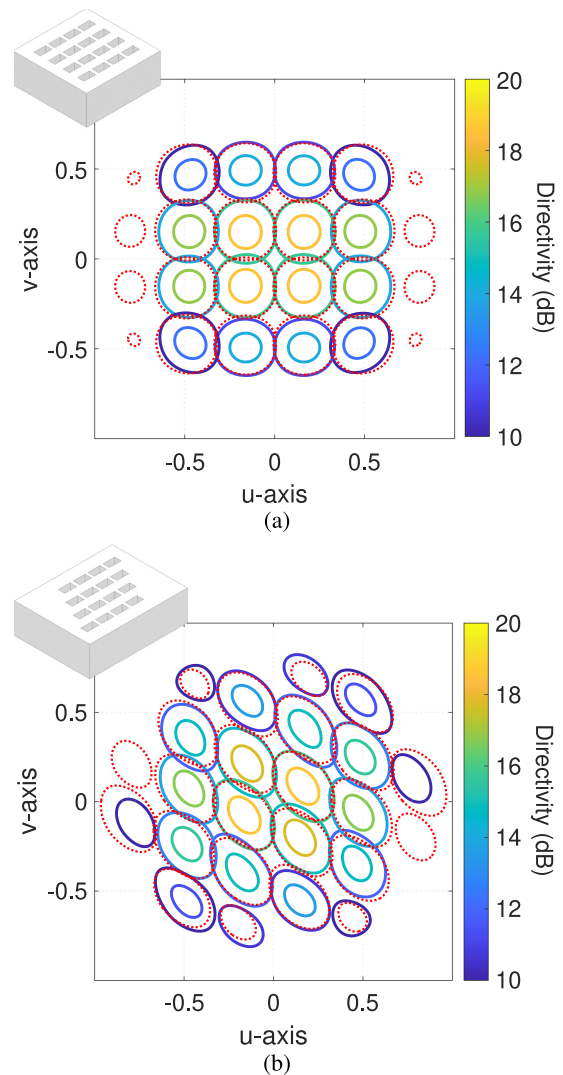


FIGURE 2. Contour plots at 1 dB and 3.9 dB below peak directivity of each beam for (a) a 4×4 square array and (b) a 4×4 diamond array, with *red dotted lines* corresponding to 3.9 dB contours of the corresponding ideal arrays (insets: ANSYS HFSS array models).

With the approach introduced in [29] and generalized here, there is no need to load array elements to improve the crossover level. The array shape is adjusted by rearranging elements as illustrated in Fig. 3a. As the phase progressions in a $N \times N$ 1D symmetric Butler matrix are given by [33]

$$\Delta\phi = \frac{(2k-1)\pi}{N}, \quad k = 1 \dots N, \quad (1)$$

the N -element linear array may be extended at both ends by repeating all elements with a phase shift of $\pm\pi$. This property was first described in [30] to reduce side lobe levels at the cost of a degraded beam crossover and is considered here to relocate elements without affecting the phase progressions required to synthesize the beams. The ports in *red* in Fig. 3a are the ports “rearranged” with a phase difference of $\pm\pi$. This phase difference can be conveniently introduced in waveguide technology with a matrix of twists at the output ports of the 2D

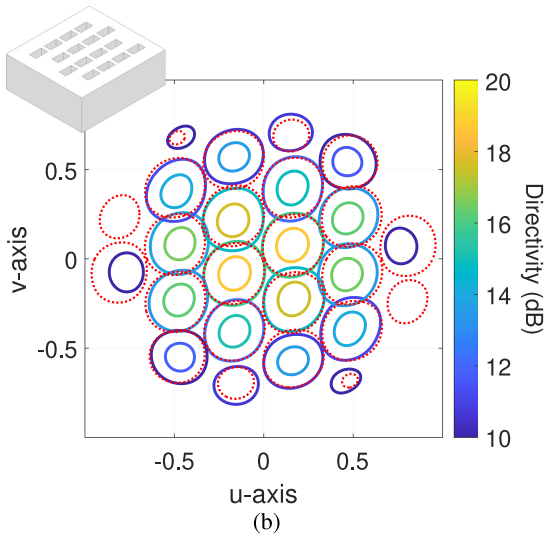
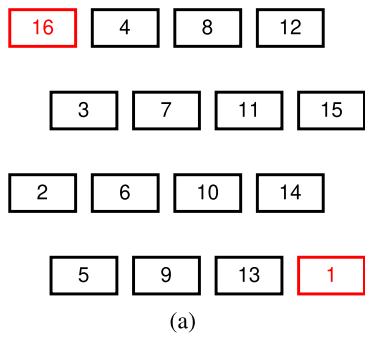


FIGURE 3. 16-element array with triangular lattice and rearranged elements: (a) array layout and (b) contour plots at 1 and 3.9 dB below peak directivity of each beam (inset: ANSYS HFSS array model).

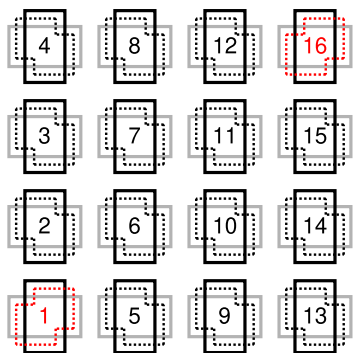


FIGURE 4. Schematic representation of a 4×4 twist layer, with twists in dashed lines, the 2D Butler matrix ports in black solid lines and the ports after the twist layer in gray solid lines. The twists with the $\pm\pi$ phase correction resulting from the symmetric design are in red.

Butler matrix: all ports in *black* have the same twist orientation while ports in *red* have a symmetric twist layout introducing a geometrical phase difference of $\pm\pi$. This approach enables a frequency-independent phase correction prior to the ports rearrangement. A schematic representation of a possible 4×4 twist layer is provided in Fig. 4. Contour plots assuming ideal connecting network and 2D Butler matrix are reported in Fig. 3b for the same open-ended waveguide configuration

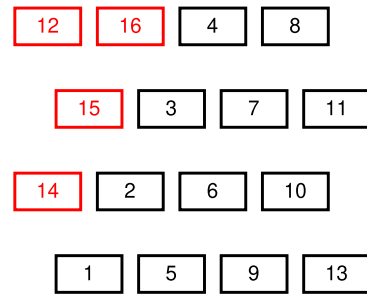


FIGURE 5. Alternative 4×4 array layout with triangular lattice and rearranged elements in red.

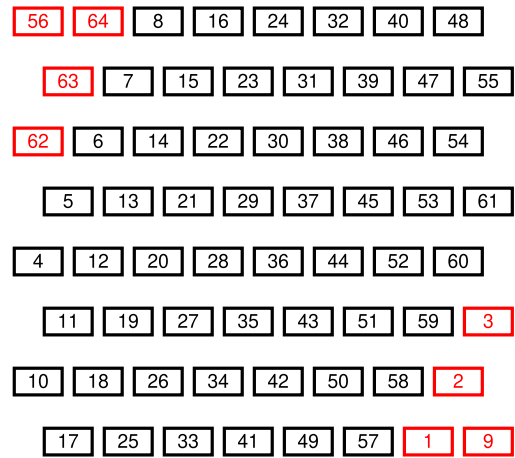


FIGURE 6. Illustration of a possible ports rearrangement and $\pm\pi$ phase correction implementation (ports in red) in the case of an 8×8 array.

as above and indicate an improvement in beam crossover by more than 1 dB with marginal impact on maximum gain. The worst-case beam crossover is -5.8 and -6.8 dB for respectively the ideal array and the full-wave array models. Note that other port rearrangement layouts are possible as long as they follow the property described above and provide a layout similar to the one illustrated in Fig. 3a, i.e. with an outer array shape essentially square, which is required to produce beams with circular contour levels. An array layout with a different rearrangement of ports is illustrated in Fig. 5 for the case of a 4×4 array. The main advantage of the layout pictured in Fig. 3a is that it has intrinsic symmetry, meaning that the top half of the array is identical to the bottom half upon rotation of 180° , thus reducing the design effort. The extension of the concept to an 8×8 array following this symmetrical rearrangement of ports is illustrated in Fig. 6.

Interestingly, assuming an array with dimensions $N \times N$, where $N = 2^n$ and $n > 1$, one can derive a general rule for the number of ports that need to be rearranged, with a symmetric twist design, in a given row k given by $R_k = (2k - 1 + (-1)^k)/4$, for $k = 1 \dots N$, following an incremental rearrangement approach where the row 1 (bottom row) has no ports rearranged as illustrated in Fig. 5. In the symmetric rearrangement case illustrated in Fig. 3a and Fig. 6, the

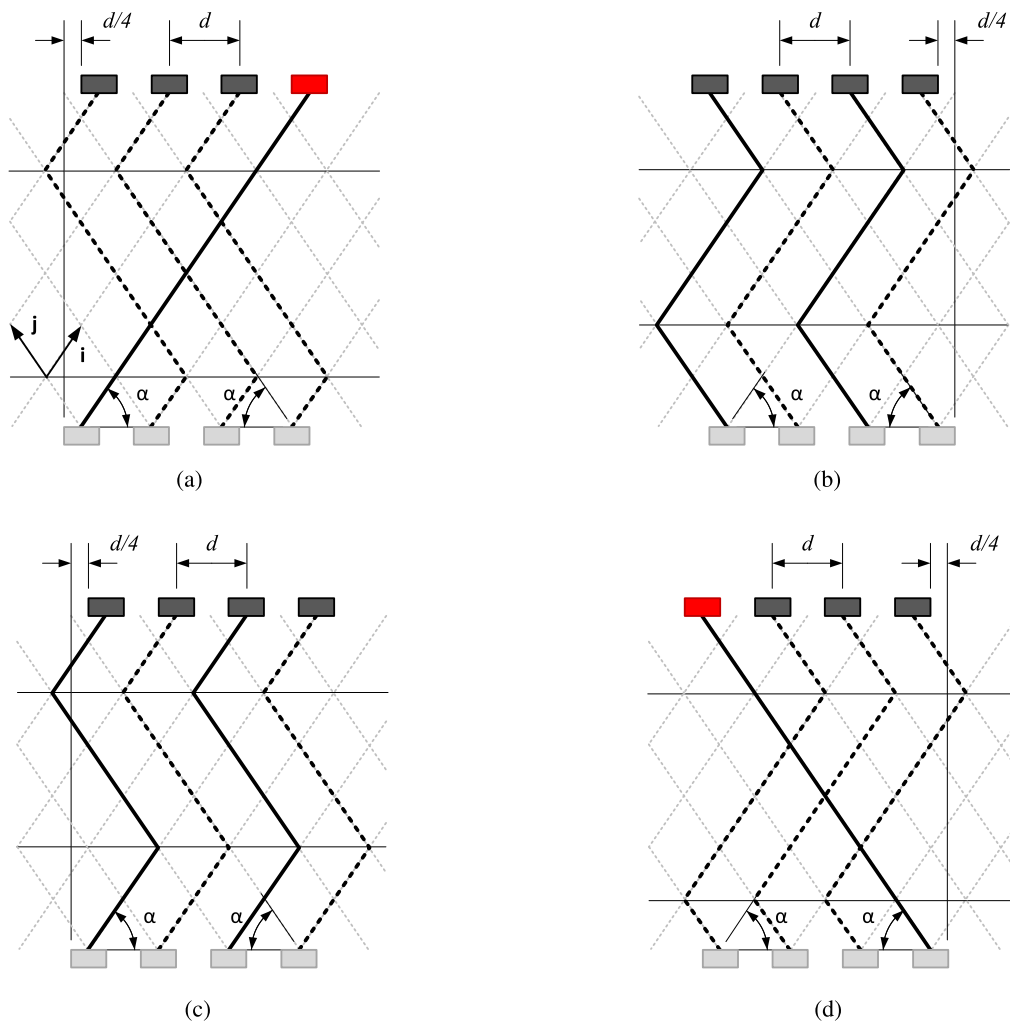


FIGURE 7. Schematic representation of the connecting network producing the array layout of Fig. 3a: (a) bottom outer row, (b) bottom inner row, (c) top inner row and (d) top outer row. Matrix ports are in gray, while array ports are in black, with rearranged array ports highlighted in red. The different layers are represented by solid lines and dashed lines.

number of ports that need to be rearranged in row k is given by $S_k = |N/4 - R_k|$, $k = 1 \dots N$. This shows that the number of ports to be rearranged is always equal to $N^2/8$, thus the design complexity of the proposed connecting network remains low. A possible layout of connecting network is detailed in the following section.

B. TRANSMISSION LINES LAYOUT

Equalizing the transmission line lengths is essential to maintain broad band operation with the connecting network. In the case of flexible transmission lines, such as coaxial cables, this can be quite straightforward. However, implementing the connecting network in the same technology as the 2D Butler matrix, using waveguide transmission lines, is preferred for higher integration. Obviously, minimizing the length of the connecting network is also important, otherwise the benefits of using a 2D BFN would be lost.

We introduce here a systematic approach for the design of a connecting network based on the symmetric array layout of Fig. 3a. The two-fold rotational symmetry requires the rows

of array element ports to be shifted by $\pm d/4$ with reference to the matrix ports along the horizontal axis. The transmission line driving the design, having the longer physical length, is the one of the rearranged elements. These waveguides are set to connect the corresponding matrix and array ports in a straight line, neglecting bends that are required in a real implementation. That straight line defines an angle α with respect to the plane of the matrix and the array, as illustrated in Fig. 7. Introducing the system of skew coordinates (i, j) where \mathbf{i} , \mathbf{j} are the basis vectors such that $\|\mathbf{i}\| = \|\mathbf{j}\| = d/(2 \cos \alpha)$ and $\widehat{\mathbf{i}} \cdot \widehat{\mathbf{j}} = \pi - 2\alpha$, the ℓ_1 norm of any vector connecting a matrix port to a corresponding array port is constant and equal to $(4N - 3)/2$ in that reference frame. A design of the transmission lines following the ℓ_1 norm provides the desired equal-length property. This is illustrated in Fig. 7. Alternative transmission line layouts, following the same ℓ_1 norm approach and satisfying also the equal-length condition, are possible. The one illustrated in Fig. 7 is meant to reduce the transverse dimension of the connecting network along the horizontal axis.

The rows with rearranged ports, highlighted in *red* in Fig. 7, require line crossings. They can be implemented using a two-layer design, schematically represented using *solid lines* and *dashed lines* in Fig. 7. In the previous design reported [29], a transition stage is added to reduce the narrow wall dimension of the waveguides and facilitate crossings between the different paths of a same row. For the two inner rows (Fig. 7b and Fig. 7c), there is effectively no need of a two-layer design, as the transmission line design is constrained by the outer rows. Indeed, if one can design the 3 adjacent lines that need to be on the same layer in the two outer rows (Fig. 7a and Fig. 7d), a similar design can be implemented for the 4 lines in the inner rows (Fig. 7b and Fig. 7c). Ideally, one would like the angle α to be as small as possible to reduce the length of the connecting network. However, with the small port-to-port spacing $d \approx 0.7\lambda_0$ considered here, where λ_0 is the wavelength in free space, the waveguides are already close to cut-off frequency. A trade-off is required between compactness and performance. A ridge waveguide design can be used to further reduce the length of the connecting network. This is illustrated through a specific K-band design in the following section.

III. CONNECTING NETWORK IN K-BAND

A. DESIGN DESCRIPTION

The connecting network described in this paper is designed to match a 16×16 2D Butler matrix with center frequency 19.55 GHz, adapted from the design at 22 GHz reported in [16] and using the 2D components described in [18]. The details of the 2D Butler matrix design are provided in previous works and are not repeated here, as the focus of this paper is on the connecting network. The design operates within the portion of the K-band allocated to satellite communication down-link. The matrix ports have the following parameters: $a = 8.83$ mm, $b = 4.89$ mm and $d = 9.9$ mm. In the previous connecting network design reported in [29], a symmetric twist was used [34]. This required to add a transition section at both ends of the connecting network to reduce the narrow wall dimension of the waveguides and displace them to enable crossing between lines. In this paper, an offset twist, adapted from the design in [35], [36], is introduced to suppress the transition stage, resulting in a more compact design. The offset twist parameters are defined in Fig. 8. Note that the CAD drawings include milling radii, the twist cavity being milled along the longitudinal direction, while the connecting network waveguides are milled along the transverse direction.

The twist design makes the transition from the 2D Butler matrix ports to the connecting network waveguides with dimensions $a_r = 8.5$ mm and $b_r = 3.75$ mm. The design is tuned such that $b_r < a/2$, thus two waveguides with symmetric offset can cross paths, while maintaining a separation of 1.33 mm. The symmetric offsets are obtained rotating the twist by 180° , thus providing the same insertion phase in both offset positions. Also, $a_r < a$ to provide sufficient wall thickness between waveguide transmission lines once inclined

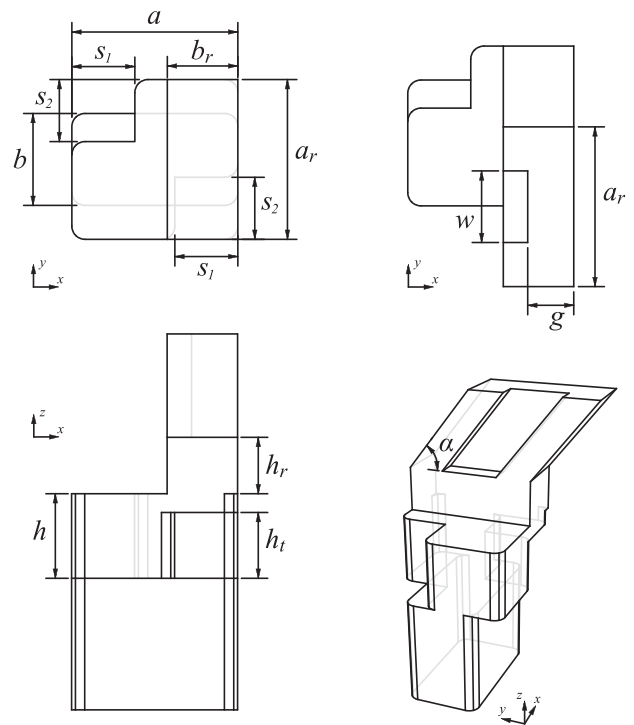


FIGURE 8. Design parameters of the proposed offset twist and transition to the inclined single ridge waveguide of the connecting network.

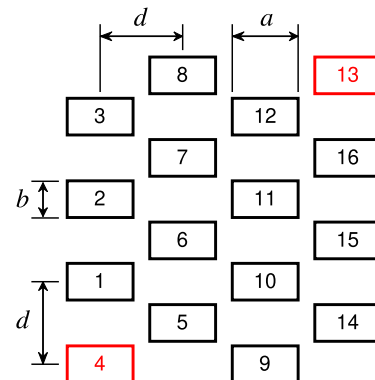


FIGURE 9. Design parameters of a 4×4 array layout with triangular lattice and rearranged elements (in red).

by the angle α . In this design, $\alpha = 52^\circ$, resulting in a minimum wall thickness of about 1.1 mm between two inclined waveguides. Because of the asymmetric input and output twist port designs, slightly asymmetric corner-cuts are introduced to improve the response, with dimensions s_1 and s_2 as well as a partial cut-out on the side of the offset waveguide, h_t . The height of the twist is the same for all transmission lines, $h = 4.5$ mm, as well as the distance to the inclined waveguide, $h_r = 3$ mm. A single ridge waveguide design is introduced to lower the cut-off frequency of the inclined waveguides, with parameters $w = 3.81$ mm and $g = 2.45$ mm. Note that those dimensions are defined before the inclination by the angle α (Fig. 8). The actual cross-sectional dimensions of the

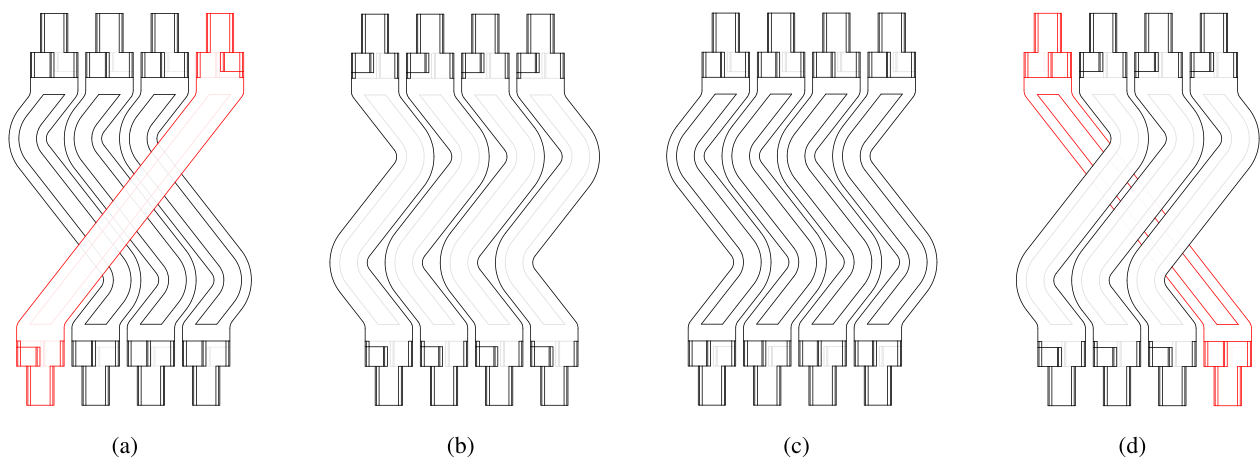


FIGURE 10. Connecting network transmission lines and twist layers producing the array layout of Fig. 9: (a) outer left column, (b) inner left column, (c) inner right column and (d) outer right column. The transmission lines of the rearranged ports with a phase correction of $\pm\pi$ are highlighted in red.

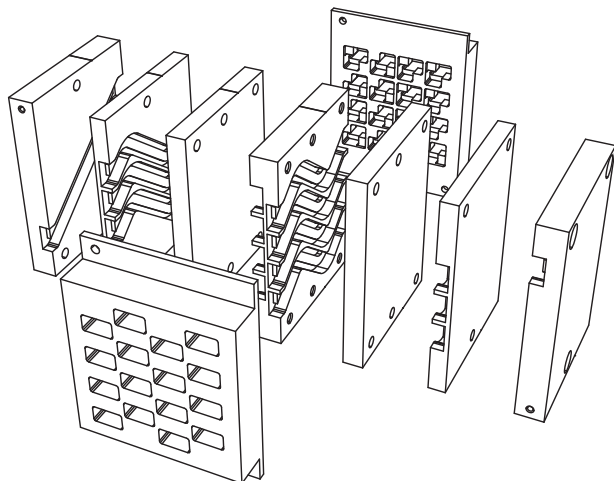


FIGURE 11. Exploded CAD view of the multiple parts constituting the 16×16 connecting network designed at 19.55 GHz.

single ridge design are obtained multiplying those geometric parameters by $\sin \alpha$.

With this offset twist replacing the transition layers in [29], the port rearrangement is done along the y -axis rather than x -axis as discussed in Section II. This leads to the array layout reported in Fig. 9, using the same design parameters as previously defined, but with a different arrangement of ports. One layer of twists is used only as transition, meaning that all twists are identical, while the second layer is used to introduce the desired phase correction of $\pm\pi$. The details of the different columns of transmission lines are provided in Fig. 10. The rearranged ports are highlighted in red. The bottom twist layer has all twists identical, except for the rotation by 180° to enable crossing, while the top twist layer has symmetric twists for the rearranged ports. The introduction of the bends for matching purposes slightly affects the insertion phase of the transmission lines. The ridge waveguide design of the rearranged ports is adjusted to correct for this phase variation, with $a_r = 8.5$ mm, $b_r = 3.65$ mm, $w = 3.68$ mm

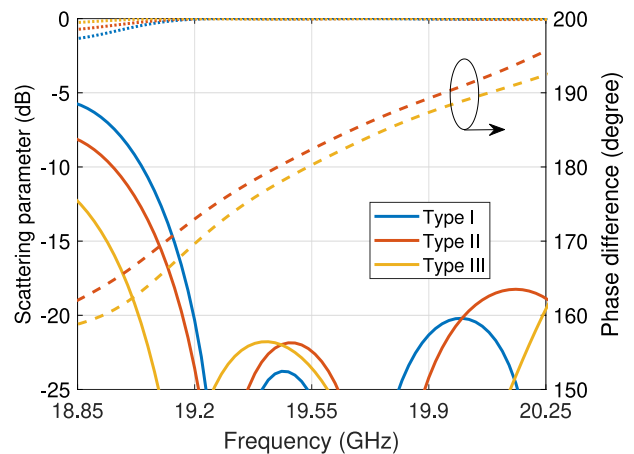


FIGURE 12. Scattering parameters of the 3 types of transmission lines required for the 16×16 connecting network designed at 19.55 GHz. Reflection (S_{11}) and transmission (S_{21}) coefficients in solid lines and dotted lines, respectively, and phase differences with reference to the type I transmission line in dashed lines.

and $g = 2.41$ mm. To improve the overall response, the twist design was optimized for each type of transmission line. The rearranged port twists, corresponding to the transmission line type I, have the following parameters: $s_1 = 3.2$ mm, $s_2 = 3.47$ mm and $h_t = 3.4$ mm. The crossing lines on the same column as the rearranged ports, which are all identical and referred to as transmission line type II, have the following parameters: $s_1 = 3.1$ mm, $s_2 = 3.5$ mm and $h_t = 3.4$ mm. The lines in the inner columns, which are also all identical and referred to as transmission line type III, have the following parameters: $s_1 = 3.35$ mm, $s_2 = 3.3$ mm and $h_t = 3.5$ mm. The designs were optimized to reach a return loss better than 20 dB over a bandwidth of 700 MHz centered at 19.55 GHz (19.2–19.9 GHz), corresponding to the operating bandwidth of the 2D Butler matrix reported in [17]. The implementation of the connecting network is done assembling the 9 parts illustrated in Fig. 11. The equal-length transmission line section is composed of 7 parts, while the remaining 2 parts are the twist

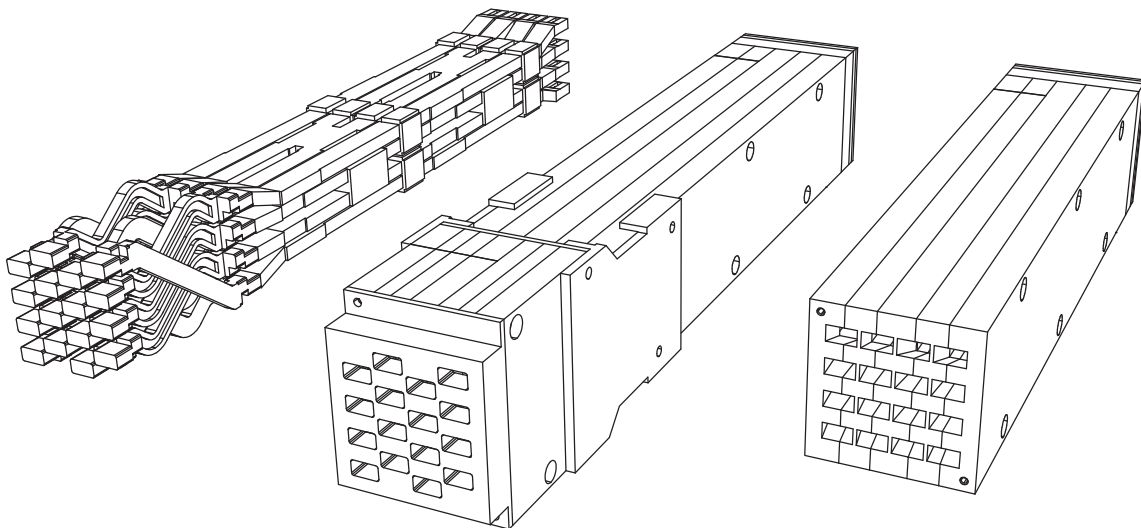


FIGURE 13. CAD view of the developed connecting network and 2D Butler matrix assembly (center), and corresponding inner waveguide paths (left), compared to the 2D Butler matrix alone (right). The connecting network is designed as a separate part to be assembled with a 2D Butler matrix [16], [17].

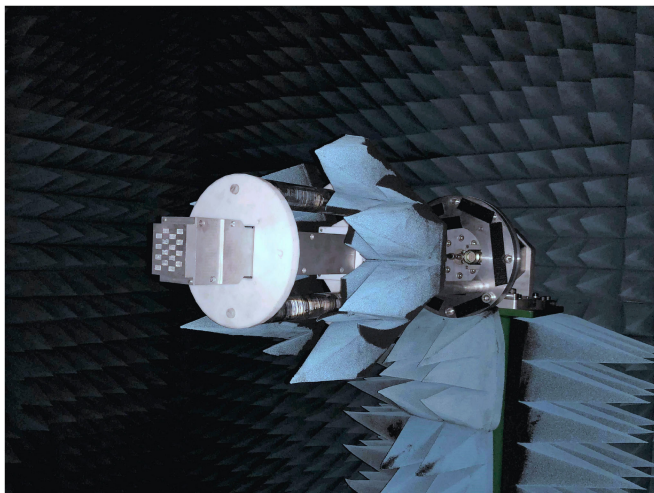


FIGURE 14. Assembled 16×16 connecting network and 2D Butler matrix under test in the anechoic chamber at KTH.

layers at both ends of the connecting network. The two twist layers have a thickness of 11.5 mm, while the transmission lines section has a length of 47.18 mm, resulting in a total length of 70.18 mm. The previous design reported in [29] and centered at 22 GHz was 100 mm long, thus demonstrating the benefit of the approach described here with the offset twists, corresponding to a length reduction of about 40% for similar in-plane dimensions. The simulation results obtained with ANSYS HFSS are reported in Fig. 12 for the 3 types of transmission lines. The insertion phase differences are formulated with reference to the rearranged port transmission line (type I) and are reported with *dashed lines* in Fig. 12. The results indicate that all transmission line types operate well over the targeted frequency band. The bandwidth is limited at the lower end by the cut-off of the operating fundamental

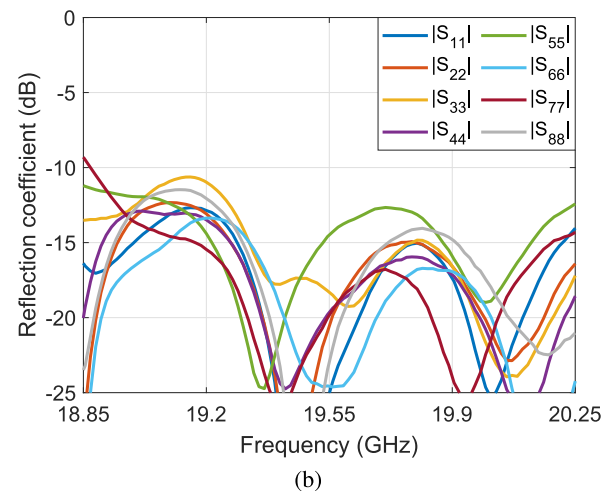
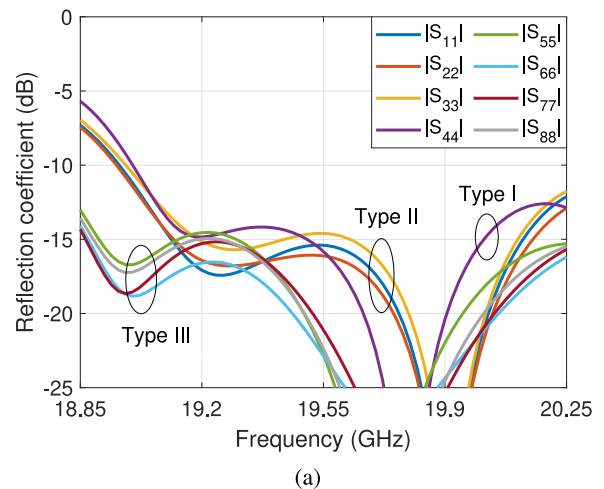
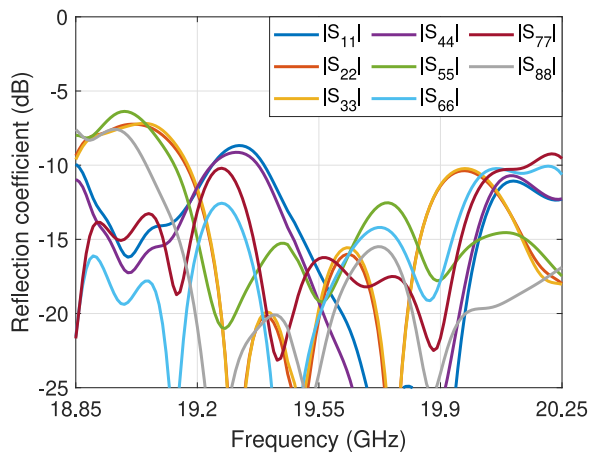
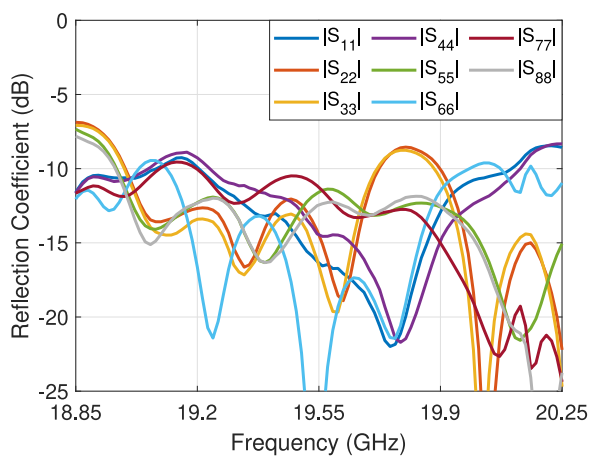


FIGURE 15. Reflection coefficients of the 16×16 connecting network with waveguide-to-coaxial connectors on the input and open-ended waveguides on the output: (a) simulations and (b) measurements.



(a)



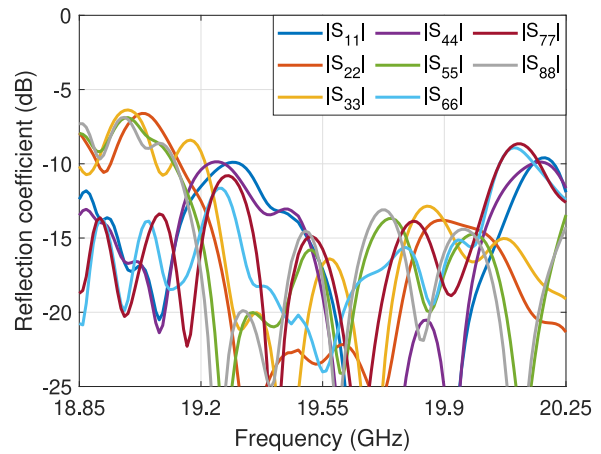
(b)

FIGURE 16. Reflection coefficients of the 16×16 2D Butler matrix with waveguide-to-coaxial connectors on the input and open-ended waveguides on the output: (a) simulations and (b) measurements.

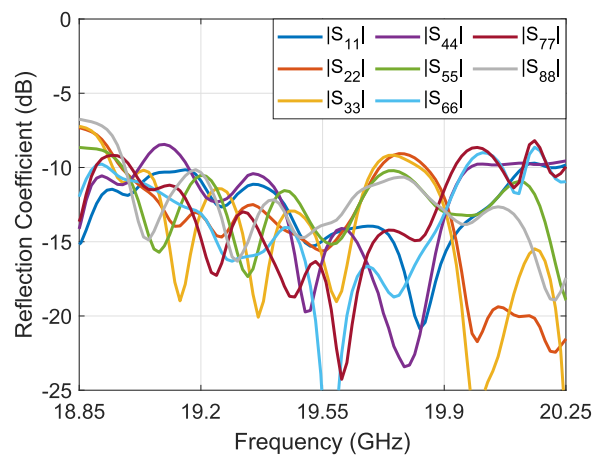
mode. A worst-case phase difference error of $\pm 10^\circ$ around the desired 180° is obtained over the frequency band 19.2–19.9 GHz. The phase difference between transmission line types II and III is stable over frequency and below 3° . This is because the dispersion is mostly introduced by the bends that are present in the line types II and III but not in the line type I. Interestingly, there are only two of those lines in the considered 4×4 matrix, and their impact on the full array response over frequency is expected to be limited. For larger arrays, it may be considered to also include the bends in the line type I to minimize differences. This would require adapting the design procedure accordingly, still following an approach similar to the one described in this paper. The resulting design is expected to be less dispersive, at the expense of a less compact connecting network.

B. EXPERIMENTAL VALIDATION

In this section, the validation of the proposed connecting network combined with a 16×16 2D Butler matrix is discussed.



(a)



(b)

FIGURE 17. Reflection coefficients of the combined connecting network and 2D Butler matrix with waveguide-to-coaxial connectors on the input and open-ended waveguides on the output: (a) simulations and (b) measurements.

The prototype is designed to enable the measurement of the 2D Butler matrix with and without the connecting network for comparison. A CAD view of the overall assembly is provided in Fig. 13, also including an illustration of the inner waveguide electrical paths. The connecting network is small compared to the 2D Butler matrix (211.69 mm long, excluding the coaxial-to-waveguide transitions for test purposes), thus maintaining the benefits of the 2D beamforming approach. The mechanical design, and in particular the inclusion of screws, leads to an increase of the in-plane dimensions (62 mm \times 54 mm for the connecting network compared to 48 mm \times 48 mm for the 2D Butler matrix), but this is considered marginal as the critical dimension remains the length of the device. A picture of the prototype under test in the anechoic chamber at KTH Royal Institute of Technology, Stockholm, Sweden, is provided in Fig. 14. Coaxial-to-waveguide transitions with a length of 14.5 mm are added, integrating modified HPC1440-02 SMA connectors [16], [17]. The simulated and measured reflection coefficients of the connecting network alone are reported in

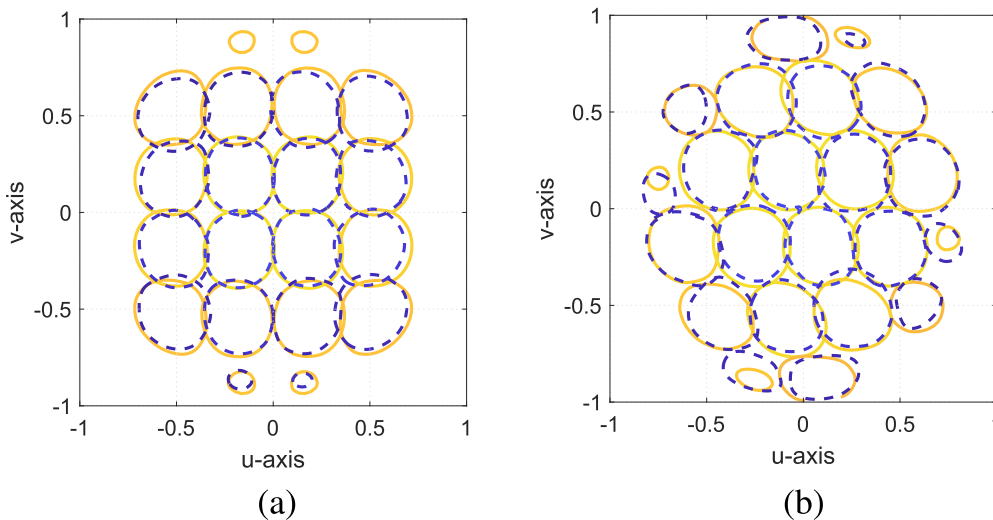


FIGURE 18. Contour plots at 3.9 dB below peak directivity of the 16 normalized beams generated at 19.55 GHz by (a) the 16×16 2D Butler matrix alone and (b) the 16×16 2D Butler matrix with the connecting network (simulated results in solid yellow lines and measured results in dashed blue lines).

Fig. 15. Similar results are reported in Fig. 16 for the 2D Butler matrix alone. Results of the combined 2D Butler matrix and connecting network are provided in Fig. 17. Note that only half of the ports are reported for readability, taking advantage of the symmetric design.

Compared to the simulated results in Fig. 12, the reflection coefficients of the connecting connector prototype alone are degraded to -14.6 dB in simulation and -14.3 dB in measurement, at the design frequency. This is because open-ended waveguides are used as radiating elements, and their mismatch to free-space dominates the return loss figure. The results are stable over the frequency range of interest, with measured values below -11 dB. Some stronger variations and a down-shift in frequency of the resonances of approximately 2% from about 19.8 to 19.4 GHz are observed when comparing simulation and measurement. Those are likely due to manufacturing tolerances and assembly errors. The prototype was not designed for guided wave characterization, and only one side was adapted to interface with coaxial-to-waveguide transitions. For this reason, only return loss values can be reported. The reflection coefficients of the 2D Butler matrix alone in Fig. 16 indicate a value of -16.3 dB and -11.5 dB at the design frequency, in simulation and measurement, respectively. These values degrade to -8.7 dB and -8.5 dB, respectively, within the operating frequency range 19.2–19.9 GHz, confirming the measurements are in line with predictions, also with a similar downshift in frequency for some of the parameters. The worst-case is observed for the edge elements (ports 1 to 4), indicating edge effects have a non-negligible impact on performance due to the small ground plane size around the open-ended waveguides. Note that these results are also in line with previously reported experimental data for a 4×4 2D Butler matrix in K-band [16]. The results combining the 2D Butler matrix and the designed connecting network

in Fig. 17 show a similar trend, confirming that the return loss is mostly driven by the performance of the Butler matrix. At the design frequency, the worst-case reflection coefficient is -15.7 dB and -13.9 dB in simulation and measurement, respectively. Over the considered frequency bandwidth, the values degrade to -9.2 dB and -8.8 dB, respectively, in line with the performance of the matrix alone.

Finally, contour plots of the multiple fixed beams generated by the 2D Butler matrix alone and the matrix combined with the proposed connecting network are reported in Fig. 18 at the design frequency, 19.55 GHz. Simulated and measured results are overlaid in the (u, v) space. The full-wave models in ANSYS HFSS account for the coupling between elements and the finite size of the array ground plane. Overall, good agreement is found between simulated and measured data. The beam crossover level of the 2D Butler matrix alone is -7.3 dB and -7.4 dB in simulation and measurement, respectively. These values improve to -5.9 dB and -6.2 dB, respectively, by adding the connecting network. Similar contour plots are reported in Fig. 19 at both 19.2 and 19.9 GHz, confirming the stability of the design over the frequency bandwidth. The expected triangular lattice and associated gain roll-off improvement are confirmed when using the proposed connecting network. Some deviations between the measured and simulated results are observed, which are attributed to manufacturing and assembly errors. The results of the Butler matrix alone show better agreement. This is because the mechanical design is such that most of the waveguides are cut through their E-plane, with minimal impact on electric currents. This approach cannot be implemented in the case of the connecting network. For this reason, larger deviations are observed, and in particular some beam pointing error for the most scanned beams. One may consider alternative manufacturing techniques, such as additive layer manufacturing or

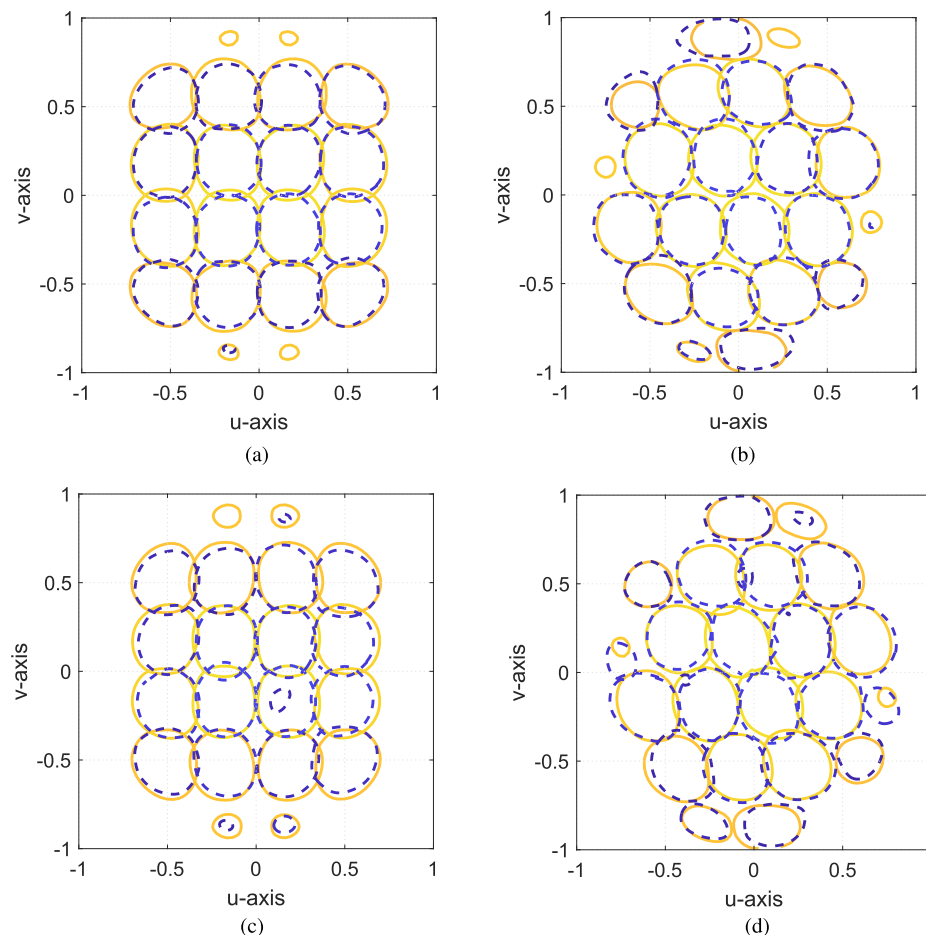


FIGURE 19. Contour plots at 3.9 dB below peak directivity of the 16 normalized beams generated at 19.2 GHz (top) and 19.9 GHz (bottom) by the 16×16 2D Butler matrix alone (left) and the 16×16 2D Butler matrix with the connecting network (right) (simulated results in solid yellow lines and measured results in dashed blue lines).

diffusion bonding, to improve the performance of this component. Overall, the agreement remains fairly good for a first proof-of-concept.

IV. CONCLUSIONS

Connecting networks, modifying standard 2D Butler matrices to generate a triangular lattice of beams, have been thoroughly discussed in this paper. A systematic design procedure for the transmission lines layout has been proposed and an implementation in waveguide technology using offset twists has been described, which reduces the overall length of the structure. The proposed design is generic and can be extended to any orthogonal BFN. Numerical results indicate an improvement ranging between 1 and 1.5 dB on the gain roll-off, while maintaining the orthogonality of the structure, resulting in low losses.

The concept was validated through a specific design, compatible with a 16×16 2D Butler matrix, with center frequency 19.55 GHz. A good trade-off between compactness and performance was found. The final design, including the transmission lines and the twist layers, is 70 mm long. For comparison, the 2D Butler matrix is 226 mm long, meaning

that the improvement in beam crossover has a rather limited impact on the overall dimensions of the device. The benefits of a 2D beamforming approach are thus preserved. The experimental data, with an open-ended waveguide array configuration, provides acceptable return loss over a fractional bandwidth of about 3 to 4%. In fact, the results are limited by the performance of the Butler matrix itself, with values in line with previously reported experimental data. It is anticipated that the performance may be improved with suitable upgrades to the 2D Butler matrix design. Measured radiation patterns indicate an improvement of about 1.2 dB on the beam crossover, confirming the expected benefits observed in simulation.

Future works will investigate the feasibility of a more integrated design, to reduce further the dimensions of the BFN. An extension to larger matrices may be considered. There is also some interest to assess the concept at higher frequencies, where dimensions are less of an issue and low loss designs are desirable. This highly efficient antenna solution is of interest for broadband communication systems on-board small space platforms and unmanned aerial vehicles with limited power supply. It may also find applications in 5G/6G terrestrial systems.

REFERENCES

- [1] J. Blass, "Multidirectional antenna: A new approach to stacked beams," in *Proc. IRE Int. Conv. Rec.*, part 1, 1960, pp. 48–50.
- [2] P. Chen, W. Hong, Z. Kuai, and J. Xu, "A double layer substrate integrated waveguide blass matrix for beamforming applications," *IEEE Microw. Wireless Compon. Lett.*, vol. 19, no. 6, pp. 374–376, Jun. 2009.
- [3] J. Butler, "Beam-forming matrix simplifies design of electronically scanned antennas," *Electron. Des.*, vol. 9, pp. 170–173, Apr. 1961.
- [4] J. Shelton and K. Kelleher, "Multiple beams for linear arrays," *IRE Trans. Antennas Propag.*, vol. AP-9, no. 2, pp. 154–161, Mar. 1961.
- [5] M. Ansari, H. Zhu, N. Shariati, and Y. J. Guo, "Compact planar beamforming array with endfire radiating elements for 5G applications," *IEEE Trans. Antennas Propag.*, vol. 67, no. 11, pp. 6859–6869, Nov. 2019.
- [6] J. Nolen, "Synthesis of multiple beam networks for arbitrary illuminations," Ph.D. dissertation, Dept. Radio Division, Bendix Corp., John Hopkins University, Baltimore, MD, USA, Apr. 1965.
- [7] N. J. G. Fonseca, "Printed S-band 4×4 Nolen matrix for multiple beam antenna applications," *IEEE Trans. Antennas Propag.*, vol. 57, no. 6, pp. 1673–1678, Jun. 2009.
- [8] T. Djerafi, N. J. G. Fonseca, and K. Wu, "Broadband substrate integrated waveguide 4×4 Nolen matrix based on coupler delay compensation," *IEEE Trans. Microw. Theory Techn.*, vol. 59, no. 7, pp. 1740–1745, Jul. 2011.
- [9] F. Doucet *et al.*, "Shaped continuous parallel plate delay lens with enhanced scanning performance," *IEEE Trans. Antennas Propag.*, vol. 67, no. 11, pp. 6695–6704, Nov. 2019.
- [10] O. Quevedo-Teruel *et al.*, "Glide-symmetric fully-metallic Luneburg lens for 5G communications at Ka-band," *IEEE Antennas Wireless Propag. Lett.*, vol. 17, no. 9, pp. 1588–1592, Sep. 2018.
- [11] Q. Liao, N. J. G. Fonseca, and O. Quevedo-Teruel, "Compact multi-beam fully-metallic geodesic Luneburg lens antenna based on non-Euclidian transformation optics," *IEEE Trans. Antennas Propag.*, vol. 66, no. 12, pp. 7383–7388, Dec. 2018.
- [12] H. Lu, Z. Liu, Y. Liu, H. Ni, and X. Lv, "Compact air-filled Luneburg lens antennas based on almost-parallel plate waveguide loaded with equal-sized metallic posts," *IEEE Trans. Antennas Propag.*, vol. 67, no. 11, pp. 6829–6838, Nov. 2019.
- [13] N. J. G. Fonseca, Q. Liao, and O. Quevedo-Teruel, "Equivalent planar lens ray tracing model to design modulated geodesic lenses using non Euclidian transformation optics," *IEEE Trans. Antennas Propag.*, vol. 68, no. 5, pp. 3410–3422, May 2020.
- [14] N. J. G. Fonseca, Q. Liao, and O. Quevedo-Teruel, "Compact parallel plate waveguide half-Luneburg geodesic lens in the Ka-band," *IET Microw. Antennas Propag.*, vol. 15, no. 2, pp. 1–8, Dec. 2020.
- [15] D.-H. Kim, J. Hirokawa, and M. Ando, "Design of waveguide short-slot two-plane couplers for one-body 2-D beam-switching Butler matrix application," *IEEE Trans. Microw. Theory Techn.*, vol. 64, no. 3, pp. 776–784, Mar. 2016.
- [16] D.-H. Kim, J. Hirokawa, and M. Ando, "One-body 2-D beam-switching Butler matrix with waveguide short-slot 2-plane couplers," *IEICE Trans. Electron.*, vol. E100-C, no. 10, pp. 884–892, Oct. 2017.
- [17] T. Tomura, D. Kim, M. Wakasa, Y. Sunaguchi, J. Hirokawa, and K. Nishimori, "A 20-GHz-band 64×64 hollow waveguide two-dimensional Butler matrix," *IEEE Access*, vol. 7, pp. 164080–164088, Nov. 2019.
- [18] J. Hirokawa, D. Kim, M. Wakasa, Y. Sunaguchi, T. Tomura, and K. Nishimori, "Measurements of a 64×64 -way one-body two-dimensional beam-switching hollow-waveguide Butler matrix," in *Proc. 48th Eur. Microw. Conf.*, Madrid, Spain, Sep. 2018, Paper no. EuMC08-4, pp. 125–128, doi: [10.23919/EuMC.2018.8541758](https://doi.org/10.23919/EuMC.2018.8541758).
- [19] J. P. Shelton, "Multibeam planar arrays," *Proc. IEEE*, vol. 56, no. 11, pp. 1818–1821, Nov. 1968.
- [20] J. L. Allen, "A theoretical limitation on the formation of lossless multiple beams in linear arrays," *IRE Trans. Antennas Propag.*, vol. 9, no. 4, pp. 350–352, Jul. 1961.
- [21] W. D. White, "Pattern limitations in multiple-beam antennas," *IRE Trans. Antennas Propag.*, vol. 10, no. 4, pp. 430–436, Jul. 1962.
- [22] J. W. Locke, "Apparatus and method for the beamforming in a triangular grid pattern," U.S. Patent 5,812,089, Sep. 1998.
- [23] M. J. Maybell and G. S. Hardie, "EHF waveguide Rotman lens for reconfigurable SATCOM," in *Proc. 39th ESA Antenna Workshop*, Noordwijk, The Netherlands, Oct. 2018, pp. 1–8.
- [24] W. Rotman and R. F. Turner, "Wide-angle microwave lens for line source applications," *IEEE Trans. Antennas Propag.*, vol. 11, no. 6, pp. 623–632, Nov. 1963.
- [25] N. J. G. Fonseca, E. Girard, and H. Legay, "Doubly curved reflector design for hybrid array fed reflector antennas," *IEEE Trans. Antennas Propag.*, vol. 66, no. 4, pp. 2079–2083, Apr. 2018.
- [26] N. J. G. Fonseca, E. Girard, and H. Legay, "Design of a hybrid linear-array fed doubly curved reflector antenna with a hexagonal beam lattice," in *Proc. 13th Eur. Conf. Antennas Propag.*, Krakow, Poland, May 2019, pp. 1–4.
- [27] N. J. G. Fonseca, E. Girard, and H. Legay, "Doubly curved reflector antenna design trade-offs for a hexagonal lattice of beams," in *Proc. Int. Symp. Antennas Propag.*, Osaka, Japan, Jan. 2021, Paper no. 3D4.1, pp. 1–2.
- [28] K. K. Chan and S. K. Rao, "Design of a Rotman lens feed network to generate a hexagonal lattice of multiple beams," *IEEE Trans. Antennas Propag.*, vol. 50, no. 8, pp. 1099–1108, Aug. 2002.
- [29] N. J. G. Fonseca, S.-A. Gomanne, and J. Hirokawa, "Connecting networks for two-dimensional Butler matrices with improved aggregate gain," in *Proc. Int. Symp. Antennas Propag.*, Osaka, Japan, Jan. 2021, Paper no. 2E4-2, pp. 1–2.
- [30] J. P. Shelton, "Reduced sidelobes for Butler-matrix-fed linear arrays," *IEEE Trans. Antennas Propag.*, vol. 17, no. 5, pp. 645–647, Sep. 1969.
- [31] N. J. G. Fonseca and N. Ferrando, "Nolen matrix with tapered amplitude law for linear array with reduced side lobe level," in *Proc. 4th Eur. Conf. Antennas Propag.*, 2010, pp. 1–5.
- [32] P. Angeletti, "Multiple beams from planar arrays," *IEEE Trans. Antennas Propag.*, vol. 62, no. 4, pp. 1750–1761, Apr. 2014.
- [33] H. Moody, "The systematic design of the Butler matrix," *IEEE Trans. Antennas Propag.*, vol. TAP-12, no. 6, pp. 786–788, Nov. 1964.
- [34] A. A. Kirilenko, D. Y. Kulik, and L. A. Rud, "Compact 90° twist formed by a double-corner-cut square waveguide section," *IEEE Trans. Microw. Theory Techn.*, vol. 56, no. 7, pp. 1633–1637, Jul. 2008.
- [35] N. J. G. Fonseca, "Waveguide power divider," Eur. Pat. Appl. EP20157041, Feb. 12, 2020.
- [36] N. J. G. Fonseca, "Broadband waveguide dual-polarization four-way power divider for small passive arrays," to be published.



NELSON J. G. FONSECA (Senior Member, IEEE) received the M.Eng. degree from Ecole Nationale Supérieure d'Electrotechnique, Electronique, Informatique, Hydraulique et Télécom-munications (ENSEEIH), Toulouse, France, in 2003, the M.Sc. degree from the Ecole Polytechnique de Montreal, Quebec, Canada, also in 2003, and the Ph.D. degree from Institut National Polytechnique de Toulouse - Université de Toulouse, France, in 2010, all in electrical engineering.

He currently works as an Antenna Engineer for the Antenna and Sub-Millimetre Waves Section, European Space Agency (ESA), Noordwijk, The Netherlands. Since November 2020, he has held an Honorary Appointment as Professional Fellow at the University of Technology Sydney (UTS), Australia. His research interests include multiple beam antennas for space missions, beam-former theory and design, ground terminal antennas and novel manufacturing techniques. He has authored or coauthored more than 220 papers in peer-reviewed journals and conferences, and contributed to 26 technical innovations, protected by over 50 patents issued or pending.

Dr. Fonseca is currently serving as an Associate Editor for the *IET Microwaves, Antennas and Propagation* (MAP) and for IEEE TRANSACTIONS ON MICROWAVE THEORY AND TECHNIQUES (TMTT), and as a Topic Editor for IEEE JOURNAL OF MICROWAVES (JMW). He is also serving as the Co-Vice Chair of the newly founded IEEE MTT-S Technical Committee 29 (MTT-29) on Microwave Aerospace Systems. He has been a Board Member of the European School of Antennas (ESoA) since January 2019 and is also serving as coordinator of the ESA/ESoA course on Antennas for Space Applications, for which he was voted best Lecturer by the participants of the 2020 edition. He is the elected EurAAP Regional Delegate representing Benelux for the term 2021–2023. He received several prizes and awards, including the Best Young Engineer Paper Award at the 29th ESA Workshop on Antennas in 2007, an ESA Teamwork Excellence Award in 2020, and multiple ESA Technical Improvement Awards.



SOPHIE-ABIGAE GOMANNE was born in Portsmouth, U.K. in 1994. She received the M.Eng. degree in telecommunications engineering from Telecom Sud-Paris, Institut Polytechnique de Paris, Evry, France, and the M.Sc. degree in aerospace engineering from Ecole Polytechnique de Montréal, Quebec, Canada, both in 2018.

From 2018 to 2020, she was with the European Space Agency (ESA), Noordwijk, The Netherlands, as a Young Graduate Trainee working on the antenna model for ESA's 7th Earth Explorer mission (EE7) BIOMASS. She also worked on novel beamforming solutions, including Rotman lenses and modified Butler matrices. In 2020, she joined Hanwha-Phasor, London, U.K., as an Antenna Engineer. Ms. Gomanne was the co-recipient of an ESA Teamwork Excellence Award in 2020.



PILAR CASTILLO-TAPIA received her bachelor's and master's degrees in telecommunications engineer from the University of Zaragoza, Spain, in 2017 and 2019 respectively. She is currently pursuing her PhD degree in highly-efficient integrated millimeter band antennas at KTH Royal Institute of Technology, Sweden.

Her current research interests include lens antennas, transformation optics and metasurfaces possessing higher symmetries



OSCAR QUEVEDO-TERUEL (Senior Member, IEEE) received his telecommunication engineering degree from Carlos III University of Madrid, Spain in 2005, part of which was done at Chalmers University of Technology in Gothenburg, Sweden. He received the Ph.D. degree from Carlos III University of Madrid in 2010 and was then invited as a Postdoctoral Researcher to the University of Delft (The Netherlands). From 2010 to 2011, Dr. Quevedo-Teruel joined the Department of Theoretical Physics of Condensed Matter at Universidad Autónoma de Madrid as a Research Fellow and went on to continue his postdoctoral research at Queen Mary University of London from 2011-2013.

In 2014, he joined the Division of Electromagnetic Engineering at the School of Electrical Engineering and Computer Science at KTH Royal Institute of Technology in Stockholm, Sweden where he is an Associate Professor and Director of the Master Programme in Electromagnetics Fusion and Space Engineering. He has been an Associate Editor of IEEE TRANSACTIONS ON ANTENNAS AND PROPAGATION since 2018 and is the Founder and Editor-in-Chief of the EurAAP Journal Reviews of Electromagnetics since 2020. He was the EurAAP delegate for Sweden, Norway, and Iceland from 2018-2020 and he has been a member of the EurAAP Board of Directors since January 2021. He is a distinguished Lecturer of the IEEE Antennas and Propagation Society for the period of 2019-2021 and Chair of the IEEE APS Educational Initiatives Programme since 2020.

He has made scientific contributions to higher symmetries, transformation optics, lens antennas, metasurfaces, leaky wave antennas and high impedance surfaces. He is the coauthor of 97 papers in international journals and 160 at international conferences.



TAKASHI TOMURA (Member, IEEE) received the B.S., M.S. and D.E. degrees in electrical and electronic engineering from Tokyo Institute of Technology, Tokyo, Japan, in 2008, 2011, and 2014, respectively. He was a Research Fellow of the Japan Society for the Promotion of Science (JSPS) in 2013. From 2014 to 2017, he worked at Mitsubishi Electric Corporation, Tokyo and was engaged in research and development of aperture antennas for satellite communications and radar systems. From 2017 to 2019, he was a Specially Appointed as an

Assistant Professor at Tokyo Institute of Technology, Japan. He is currently an Assistant Professor there. His research interests include electromagnetic analysis, aperture antennas and planar waveguide slot array antennas.

Dr. Tomura received the Best Student Award from Ericsson Japan in 2012, the IEEE AP-S Tokyo Chapter Young Engineer Award in 2015, and the Young Researcher Award from IEICE Technical Committee on Antennas and Propagation in 2018. He is a Member of the IEICE.



JIRO HIROKAWA (Fellow, IEEE) received the B.S., M.S. and D.E. degrees in electrical and electronic engineering from Tokyo Institute of Technology (Tokyo Tech), Tokyo, Japan in 1988, 1990, and 1994, respectively.

He was a Research Associate from 1990 to 1996 and an Associate Professor from 1996 to 2015 at Tokyo Tech. where he is currently a Professor there. He was with the antenna group of Chalmers University of Technology, Gothenburg, Sweden, as a Postdoctoral Fellow from 1994 to 1995. His research interests include slotted waveguide array antennas and millimeter-wave antennas. He received the IEEE AP-S Tokyo Chapter Young Engineer Award in 1991; the Young Engineer Award from IEICE in 1996; the Tokyo Tech Award for Challenging Research in 2003; the Young Scientists' Prize from the Minister of Education, Cultures, Sports, Science and Technology in Japan in 2005; the Best Paper Award in 2007 and a Best Letter Award in 2009 from IEICE Communications Society; and the IEICE Best Paper Award in 2016 and 2018. He is a Fellow of IEICE.